Design and Characterization of a W-Band Micromachined Cavity Filter Including a Novel Integrated Transition From CPW Feeding Lines

Yuan Li, *Student Member, IEEE*, Bo Pan, *Student Member, IEEE*, Cesar Lugo, *Member, IEEE*, Manos Tentzeris, *Senior Member, IEEE*, and John Papapolymerou, *Senior Member, IEEE*

Abstract—This paper demonstrates a novel coplanar waveguide (CPW) to rectangular waveguide (RWG) transition and its application as an integration enabling structure for filters at W-band for the first time to the best of the authors' knowledge. In the proposed wideband transition, the CPW and RWG are integrated on one side of the substrate, while the coupling probe is patterned directly on the substrate instead of being made separately. The transition is fabricated using silicon micromachining and thick-film surface micromachining techniques with high precision, which is suitable for millimeter-wave subsystems and are easily extendable to terahertz applications compared to the existing approaches. In the proposed filter design, the metallized probes are used to couple signals from the CPW to waveguide resonant cavities, therefore, the need for waveguide input/output ports is eliminated. This significantly reduces the size of the filter by approximately 30%. The transition and filter components are optimized using Ansoft's High Frequency Structure Simulator 10 (HFSS 10). The measured response of the filter has the center frequency at 96.6 GHz, 2.9% bandwidth, and a 4.14-dB insertion loss in the passband.

Index Terms—Cavity filter, coplanar waveguide (CPW), micromachining, transition, W-band.

I. INTRODUCTION

RECENTLY, communication and satellite systems are seeking a fully integrated solution where waveguide components can be accessed through planar circuit boards such as printed microstrip and coplanar waveguide (CPW) lines. Some intrinsic obstacles in this integration effort can be tackled through the reconciliation of the many fundamental differences that exist between planar and waveguide transmission.

The rectangular waveguide (RWG) has the advantages of low loss and high power capacity. However, the traditional RWG at low frequencies is bulky, making their integration into system-on-chip geometries almost impossible. Nevertheless, the size of RWG shrinks dramatically at or above the millimeter-wave frequency range or even in terahertz frequencies [1]–[3]. Meanwhile, the losses of other compact transmission lines, such as microstrips, keep increasing when the frequency

goes up. The integration of subsystems into a packaged solution with a combination of planar and waveguide components provides advantages in terms of high performance with reduced size. For this reason, it is crucial to build an understanding of planar to waveguide transition structures and their application in microwave component designs at millimeter-wave frequencies.

In the existing approaches, the transitions [4]–[6] with conventional machining techniques are not easily adopted by micromachining, which is feasible for the integration of sub-millimeter-wave circuits. The transitions from planar waveguides to substrate integrated rectangular waveguides (SIRWs) are reported [7]–[10]. These transitions have the advantages of using a low-cost printed circuit board (PCB) process. However, they suffer the reduced Q factor due to the dielectric filling, as well as relatively large minimum slot and linewidth. In the meantime, several transitions are demonstrated using the low temperature co-fired ceramic (LTCC) technique not only from the planar waveguide to RWG [11], [12], but also from laminated waveguide to air-filled waveguide [13]. These transitions implemented with the LTCC technique provide good responses, although they are limited by using metal vias to form the cavity. In [14] and [15], the transitions from the CPW line to RWG on a silicon substrate are reported with wet and dry etching techniques. The coupling probe is fabricated separately and has to be assembled on the substrate.

In our previous research [16], a novel transition is proposed. It has the advantage of high precision and easier mass production by using silicon micromachining and thick-film surface micromachining techniques. The CPW, probes, and RWG are patterned and integrated on the same side of the substrate. In [16], the back-to-back transition is designed. The measured S-parameters are quite encouraging and the preliminary transition design is discussed.

In this paper, the comprehensive design analysis of the transition is given, as well as the parameters study; secondly, a waveguide filter that takes full advantage of this transition is demonstrated for the first time. The fabrication, experimental results, and the discussion of the two-pole filter are finally presented.

II. TRANSITION DESIGN THEORY

A. Transition Analysis

This CPW to RWG transition is shown in Fig. 1. It consists of two sections: a section from the CPW line to coaxial structure and a section from the coaxial structure to RWG. A CPW to coaxial structure transformation is simple to implement since
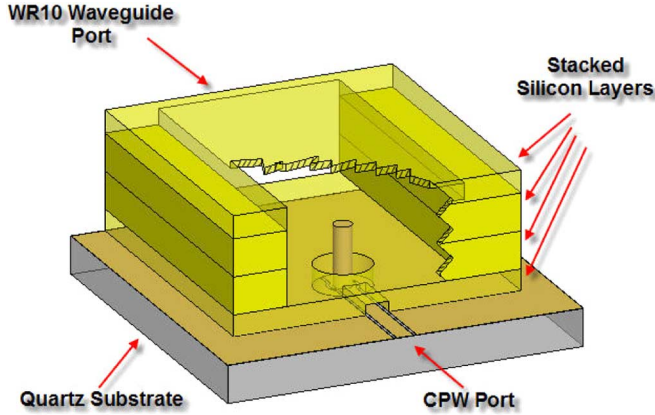
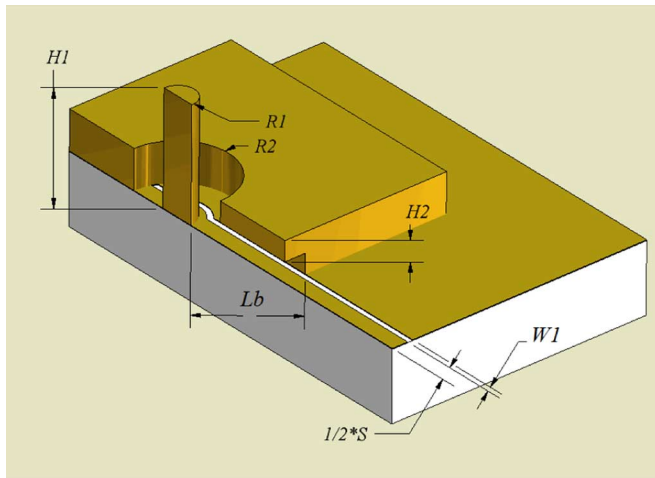Fig. 1. Schematic diagram of the transition [16].

Fig. 2. CPW and the coupling probe [16] (the transition is shown in half from the center of the broad wall, the metallized silicon sidewalls are not shown).

they both support TEM-mode (or quasi-TEM-mode) transmission; a characteristic impedance-matching geometry can be realized. From the coaxial structure to RWG, exciting the dominant TE10 mode of the RWG using a coaxial structure has been well established; the outer conductor is attached to the broad wall of the RWG, while the center conductor, the probe, extends into the RWG through an aperture at the center of the broad wall. This section can be optimized by adjusting the height of the probe in the RWG and the length of the backshort, which is the distance from the probe to the waveguide short. The impedance presented to the extending probe by the RWG is the characteristic impedance of the waveguide in parallel with the impedance introduced by the backshort. The equation to calculate the input resistance R_0 presented to the coaxial structure is given by the following equation [17]:

$$R_0 = \frac{Z_w}{2abk_0^2}|1 - e^{-2j\beta l_p}|^2 \tan^2 \frac{k_0 H}{2} \qquad (1)$$

where Z_w is the wave impedance of the waveguide at the TE10 mode, a and b are the dimensions of the waveguide, k_0 is the wavenumber, β is the propagation constant, l_p is the length of the backshort, and H is the height of the probe in the RWG. In Fig. 2, the length of the backshort is $L_b + R_1$. $H1$ denotes the

TABLE I
DIMENSIONS OF THE TRANSITION [16]

Dimensions	Value(μm)
H1	850
H2	150
R1	115
R2	400
W1	40
S	240
Lb	1000

total height of the probe including two parts: H, the height of the probe in the RWG and the height of the probe in the coaxial structure. $H2$ represents the remaining thickness of the wafer after a tunnel is etched to accommodate the CPW feeding. $R1$ is the radius of the probe. S is the width of the center conductor of the CPW. $W1$ is the width of the CPW slot.

The initial values of H and the length of the backshort can be determined by matching the impedance from the coaxial structure to the RWG. This design rule initially gives the height of the probe in the RWG over half of the waveguide height. This configuration is hard to implement due to the aspect-ratio limit in our fabrication. The height of the standard WR-10 waveguide is 1.27 mm and half of it is over 600 μm. The total height of the probe ($H1$) will be close to 1 mm including the coaxial part. To get a sufficiently good impedance matching while using a shorter probe, the aperture radius on the broad wall can be used as an additional design variable. Decreasing the probe height in the RWG is equivalent to reducing the coupling between the probe and waveguide. Different from the current probe transition in [9], an impedance transformation is taken into account [18]. This open-circuited probe transition is suitable for wideband design [19].

To compensate for the mismatching over wideband, a short-end CPW stub is introduced. It helps to improve the transition, while providing another tuning variable in the entire transition. Meanwhile, to reduce the reflection back into the coaxial structure, the aperture radius, i.e., the radius of the outer conductor of the coaxial structure, is increased to reduce the capacitive coupling between the inner and outer conductors. Consequently, it increases the characteristic impedance of the coaxial structure and thus changes the impedance matching of the transition. However, if the length of the coaxial structure is small compared to the guided wavelength, the reflection introduced in the coaxial structure only plays a minor role and can be tuned by other design variables. In this design, the length of the coaxial section is optimized to be 315 μm, which is approximately one-tenth of the wavelength at the center operating frequency. The standard WR-10 (2.54 mm × 1.27 mm) waveguide is used in the transition design, which is optimized over the entire *W*-band. The optimized dimensions are listed in Table I.

Upon the above analysis, the first-order equivalent-circuit model is given in Fig. 3 to give a better understanding of the operating mechanism of this CPW–RWG transition. In [18], an equivalent-circuit model is explained very well for a waveguide probe with a load at one end. In our study, the CPW tuning stub and the backshort are used to achieve wideband transition. In Fig. 3, the CPW tuning stub is in parallel connected to the
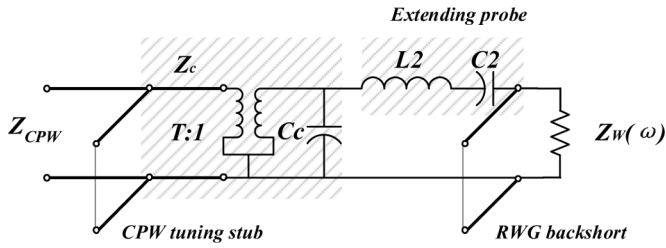
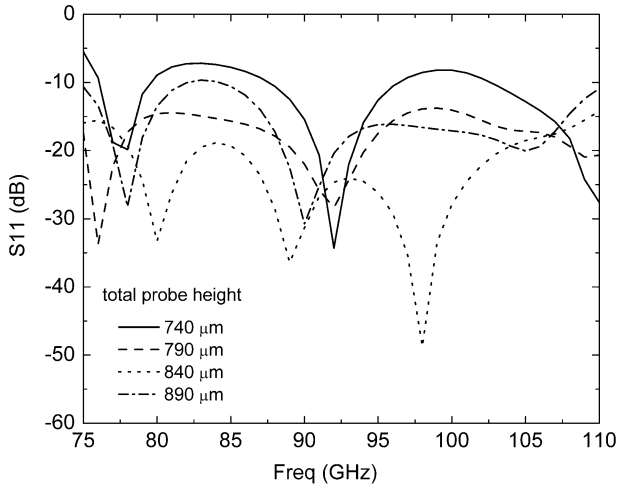Fig. 3. Equivalent-circuit model of the proposed transition.

Fig. 4. Impact of the total probe height on impedance matching (CPW tuning stub $= 400$ μm, aperture radius $= 400$ μm, coaxial section length $= 315$ μm).

Fig. 5. Impact of aperture radius (total probe height $= 840$ μm, CPW tuning stub $= 450$ μm, coaxial section length $= 315$ μm).

Fig. 6. Impact of the CPW tuning stub length (total probe height $= 840$ μm, aperture radius $= 450$ μm, coaxial section length $= 315$ μm).

Fig. 7. Impact of the coaxial section length (probe height in waveguide $= 525$ μm, aperture radius $= 400$ μm, CPW tuning stub $= 400$ μm).

coaxial structure with characteristic impedance Z_c. The transformation provided by the transformer depends on the probe height and the offset [18]. C_c denotes the capacitance between the probe and aperture. The probe in the waveguide can be modeled as a series LC circuit ($L2$ and $C2$). The waveguide backshort can also be represented as a shunt transmission line connected with the waveguide impedance. A broadband impedance transformation to match the frequency-dependent waveguide impedance into the CPW impedance is obtained through the combination of all parts. Although the standard WR-10 dimensions are used in this paper, this approach can be generalized to other RWG cross sections, especially for smaller dimensions and higher frequencies.

B. Parametric Study of the Transition

Several physical parameters are optimized to tune the impedance matching including the probe height, aperture radius, length of the tuning stub, and coaxial structure length. The height of the probe will affect not only the capacitance and the inductance, but also the transformer. The coaxial section length is studied based on the constant probe height in the RWG. The results are presented in Figs. 4–7.

III. FILTER DESIGN THEORY AND METHODOLOGY

A. Filter Design Considerations

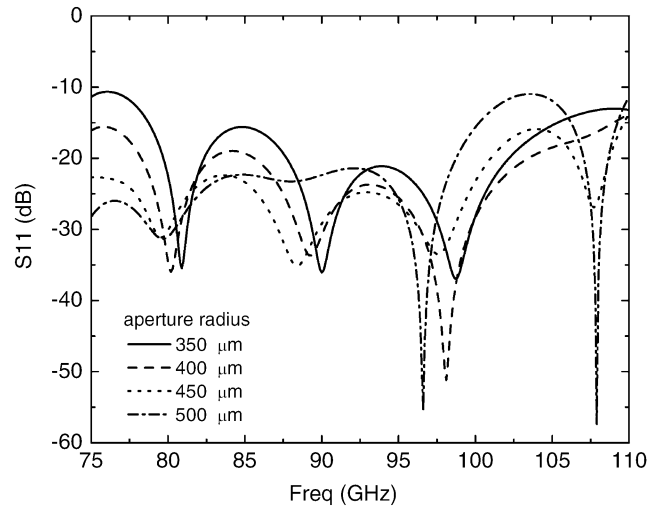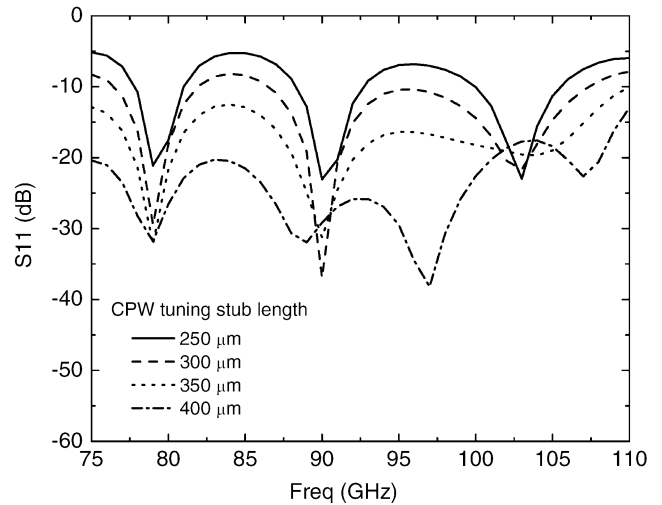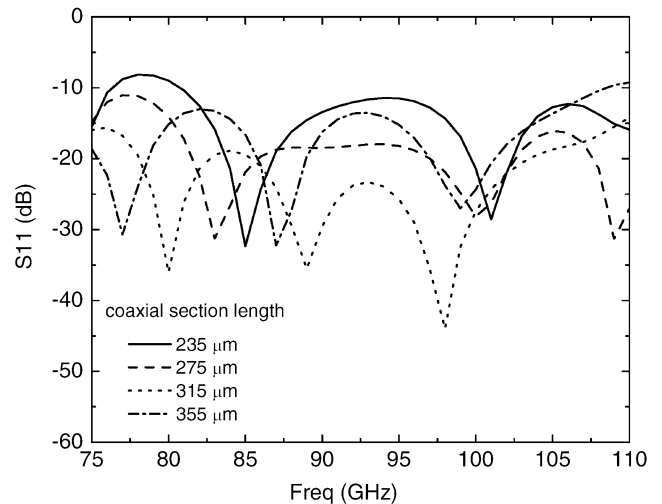The proposed second-order filter topology is shown in Fig 8. It consists of two ridge resonator structures coupled to each other. The input and output ports are produced by a direct coupling that occurs between the transition probe and the first res-
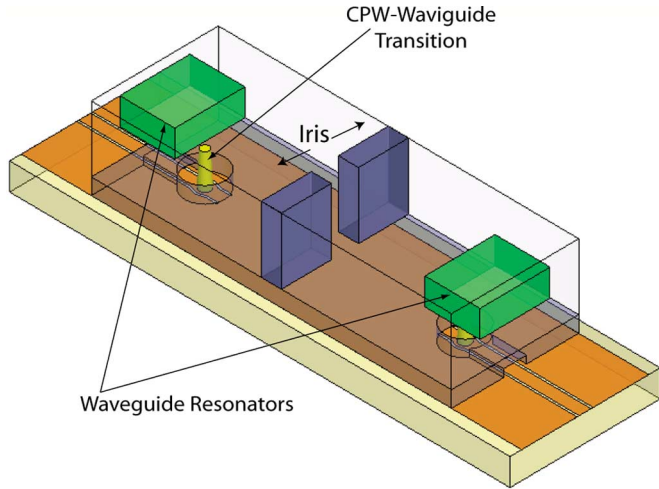
Fig. 8. Proposed filter topology. Transparent wire frame represents the enclosing metal waveguide of the filter structure.

onant mode of the structure. The standard WR-10 waveguide dimensions (2.54 mm × 1.27 mm) are utilized for the RWG. Our initial goal is to design a filter at 96.5 GHz and fractional bandwidth of 2.6% using the WR-10 dimensions. Some important filter design considerations include the size of the resonant cavity, as it dictates both the resonant frequency and proximity of the input/output coupling ports. In the case of the Chebyshev filter response, it is advantageous to minimize cross-coupling between the ports in order to increase the rejection band of the filter. The separation of the ports is increasingly critical since the transition probes will be located in a central region inside the cavity. The filter can be fully described by the resonant frequencies of the synchronous resonators with identical dimensions, the coupling factor between resonators, and the external coupling between the transition probes and the resonators. A drawing of the different layer of the filter is shown in Fig. 9.

B. Resonator Analysis and Field Distribution

The first design step is to analyze the resonance of a cavity with standard WR-10 dimensions. The resonance may be found using the fundamental equations for RWG cavities [20] given by (2) and (3). It is found that a standard RWG cavity with dimensions 2.54 mm × 2.54 mm × 1.27 mm would resonate at approximately $f_{res} = 84$ GHz. At this starting point, we are facing the need to reduce the cavity size to increase the resonant frequency while requiring the largest coupling probes separation to guarantee a good level of filter rejection

$$k_{mnl} = \sqrt{\left(\frac{m\pi}{x}\right)^2 + \left(\frac{n\pi}{y}\right)^2 + \left(\frac{l\pi}{z}\right)^2} \qquad (2)$$

$$f_{res} = \frac{ck_{mnl}}{2\pi\sqrt{\varepsilon_{eff}}}. \qquad (3)$$

One option is to adopt a ridge cavity design [21]–[24] consisting of the cavity with a solid inclusive block. This gives greater flexibility in the realization of higher resonant frequencies while increasing the separation of the coupling posts. The resonator structure is shown in Fig. 10. The cavity dimensions are a and b corresponding to the x- and z-axis. The included metal block
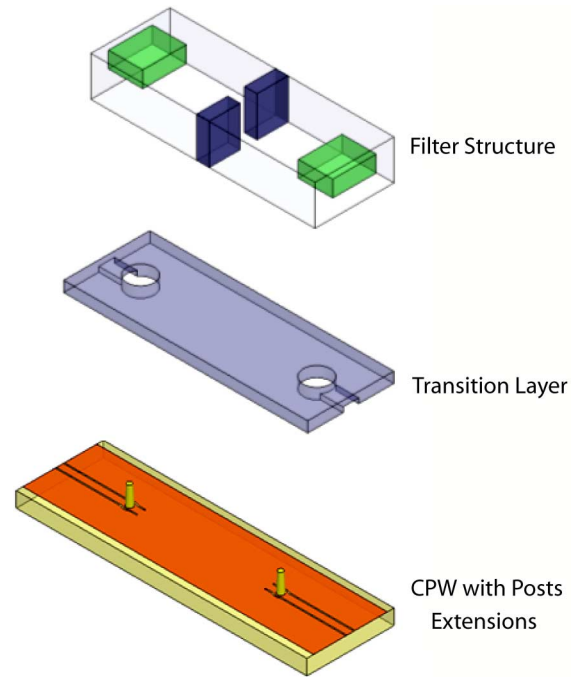

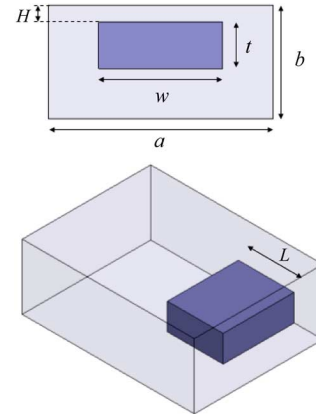Fig. 9. Different transition and filter layers.

Fig. 10. Cavity dimensions.

has a width W, thickness t, and length L in the x-, z-, and y-orientations, respectively. The thickness dimension $t = 525$ μm will be kept fixed, as it corresponds to a silicon wafer thickness. This constrain simplifies the fabrication process.

An eigenmode solution is conducted to characterize the cavity. The electric field distribution for the first resonant mode of the structure is shown in Fig. 11. The electric field pattern can be seen with strong longitudinal component along the z-axis. The field components concentrate in the region governed by the presence of the ridge component and fades with increasing $+y$. These electric field components are then used to couple to the probe of the transition placed directly below the block. The end of the waveguide with fading field strength would allow the appropriate low coupling strength to produce a selective narrowband response.

In this first analysis, the height location of the inclusive block is determined with various combinations of block sizes L and
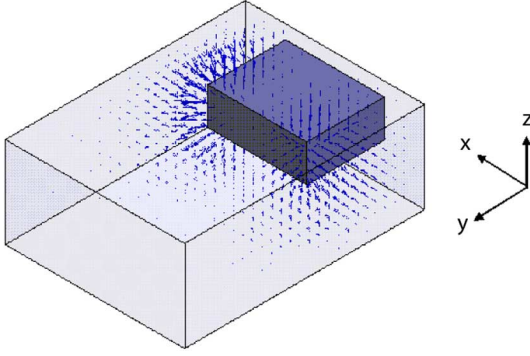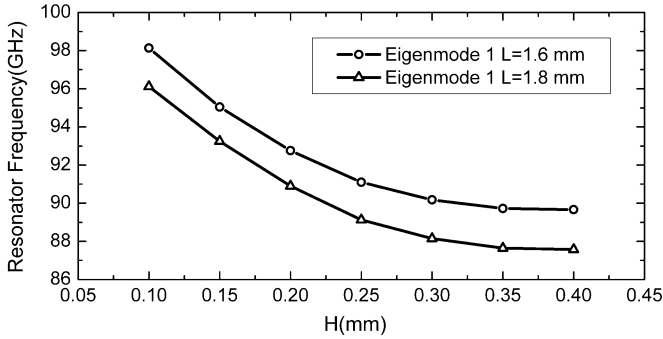
Fig. 11. Electric field pattern distribution.

Fig. 13. Cavity resonant frequency with varying L ($H = 0.2$ mm for all cases).

Fig. 12. Cavity resonant frequency with varying H ($W = 1.1$ mm for all cases).

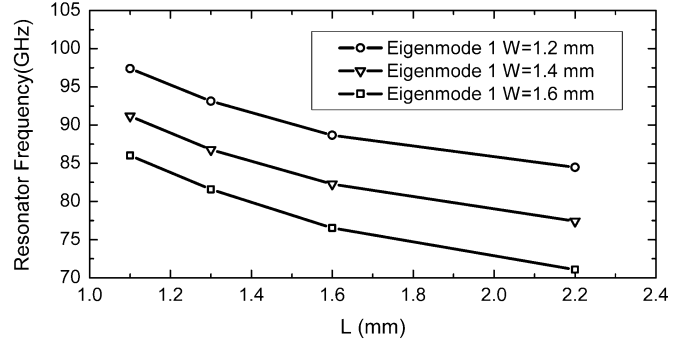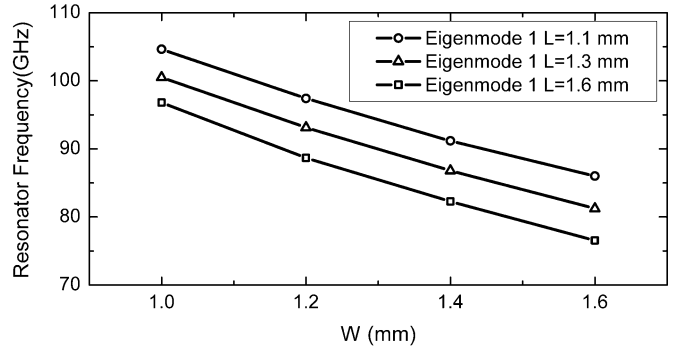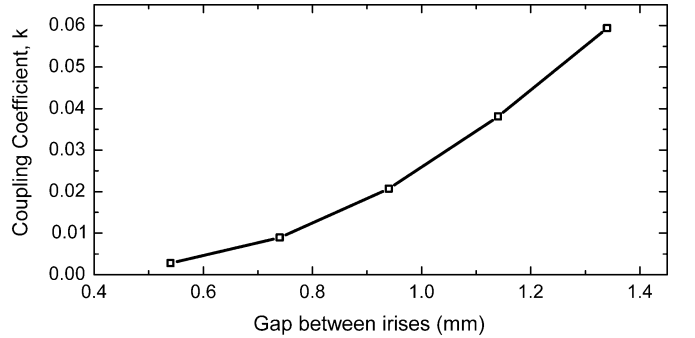Fig. 14. Cavity resonant frequency with varying W ($H = 0.2$ mm for all cases).

W. The results are shown in Fig. 12, where the resonant frequencies are plotted versus corresponding values of H, the separation from the top of the block to the ceiling of the waveguide. This procedure is repeated for varying values of L, and W, and as expected, the resonant frequency f_{res} is inversely proportional to the block dimension, as shown in Figs. 13 and 14, respectively. The presence of the internal block gives the advantages of increasing the cavity dimension along $+y$ in order to maximize port separation and still realize the increase in resonance frequency to the desired 96.5 GHz. In other words, when compared to a standard rectangular cavity, the current resonator with the internal block reduces the required size of the resonator needed for a specific center frequency. This size reduction is the advantage of evanescent mode filters, as shown in [21]–[24].

C. Coupling Between Cavities

The initial iris dimensions are designed by extracting the coupling coefficient present between resonators. The coupling coefficient is found by first placing the resonators in a weakly coupled configuration with respect to the input and output ports. The loaded resonant frequencies f_1 and f_2 are then extracted at different gap between irises. Fig. 15 shows the different coupling coefficient obtained using the standard equation for synchronous resonators

$$k = \frac{f_2{}^2 - f_1{}^2}{f_2{}^2 + f_1{}^2} \qquad (4)$$

where f_1 and f_2 are the frequency locations of each of the two resonant poles.

Fig. 15. Coupling coefficient k versus variation of the gap between irises.

IV. TRANSITION AND FILTER FABRICATION

A. CPW and Probe Fabrication

The CPW feeding and probes were fabricated on a quartz substrate with a Ti/Cu/Ti layer sputtered and patterned on one side. The SU-8 2035 was spun on the other side of the substrate and cured. The vertical probes were then patterned under the UV light and were formed after the development. To plate the CPW line, another Ti/Cu/Ti layer was sputtered as a seed layer. A negative photoresist NR9-8000 was coated with the approximate exposure to pattern the CPW slot line. The electroplating was adopted to plate a 6-μm/2-μm copper/gold to cover the sidewall of the probe and exposed feeding after the development of the NR9-8000. Finally, the seed layer was released after the negative photoresist NR9-8000 was stripped. Fig. 16 shows the CPW line, the probe, and a silicon sample in detail.
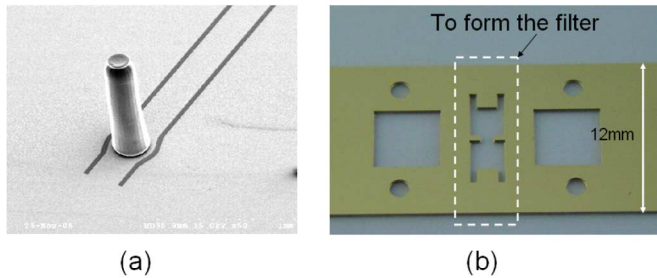
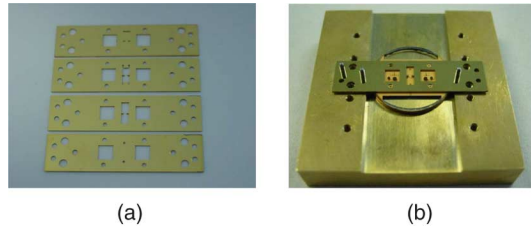Fig. 16. (a) Probe and CPW [16]. (b) One silicon layer in detail.

Fig. 17. (a) Four silicon layers to form the RWG and filter. (b) Two stacked silicon layers with a fixture.

Fig. 18. Simulation and measurement results of bandpass filter + CPW–RWG transitions.

B. Stacked Substrates

The deep-reactive iron etching (DRIE) technique was used to fabricate the silicon layers, shown in Fig. 17(a), to form the filter. The bottom layer was made by using a 300-μm-thick wafer. The two middle layers were fabricated using the 525-μm-thick wafers. The top layer was etched only 220-μm deep and released from the back with different patterns. The fixture and two silicon layers on the quartz substrate are shown in Fig. 17(b).

C. Fabrication Flow of the Silicon Wafer

The silicon wafer was cleaned and patterned using the photoresist SRP220. The STS ICP was employed to etch the patterned silicon to the desired depth. The wafer was then cleaned and the Uniaxis PECVD was used to deposit a thin silicon dioxide layer to protect the etched topside. Once the silicon dioxide was formed, the wafer was flipped and patterned on the backside using SRP220. The release of the sample was taken by using the STS ICP to etch the wafer from the backside. The diluted HF was used to remove the silicon dioxide layer. The silicon samples were sputtered using DC-Sputter with 7-μm Ti/Cu/Au.

V. SIMULATION AND MEASUREMENT RESULTS

The filter presented in this paper is simulated using Ansoft's full-wave High Frequency Structure Simulator 10 (HFSS 10). The quartz substrate used in the simulation has a dielectric constant of 3.78 and a loss tangent of 0.0002. The metal on the quartz substrate and on the silicon wafers is gold with conductivity of 4.1E7 S/m. The simulation result is reported in Fig. 18. The center frequency of the filter is 96.5 GHz with 2.6% bandwidth. The simulated insertion loss in the passband is 2.5 dB.

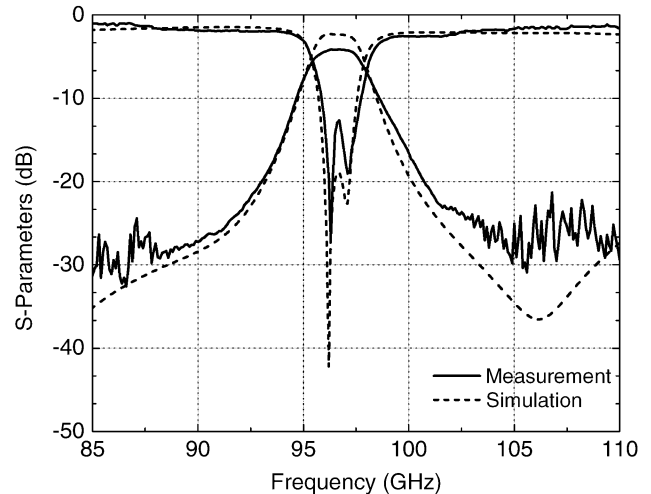The measurements at the *W*-band were taken using an Agilent Vector Network Analyzer (VNA) 8510XF. The VNA was calibrated by using the National Institute of Standards and Technology (NIST) MultiCal thru-reflect-line (TRL) algorithm. A pair of CPW probes with 250-μm pitch were used in the measurement. The measured passband insertion loss is 4.14 dB. The two poles are located at 96.3 and 97.1 GHz in the reflection loss. The measured filter has the center frequency at 96.6 GHz with the bandwidth of 2.9%. Compared to the simulated data with 2.5-dB loss in the passband, the measured filter has 1.64-dB additional loss. The bandwidth is increased by 0.3%.

The additional loss, according to our understanding, may come from the assembly tolerance, surface roughness of the silicon waveguide sidewall, and gap between the layers. The tolerance of micromachining including DRIE, photolithography, and metallization is in the level of μm or less in our class 100 cleanroom. However, the tolerance of alignment pins determined by the machine shop is in the level of mil (1/1000 in or 25.4 μm). To prevent the fight among the alignment pins during the assembly, the holes on the silicon samples are made intently larger than that of the alignment pins. A rigorous sensitivity analysis of coupled resonator filter can be found [25]. Unfortunately, we cannot directly use it since the tolerances in the assembly will affect not only the coupling, but also the impedance matching of the transition.

The simulation result in Figs. 19 and 20 shows the sensitivity of the response to the horizontal displacement of the silicon layer having the internal block. δy denotes the displacement along the CPW lines. δx denotes the displacement in perpendicular to the CPW lines. The filter is simulated while sweeping the δy and δx. The simulation shows the filter response is very sensitive to the displacement in parallel to the CPW line since the electric field is changed in this direction through the presence of the probe that is right below the block and close to the edge. To reduce the loss from assembly, a nonstandard waveguide with less height will be helpful. It will not only reduce the necessitated layers, but also simplify the transition design since the waveguide impedance is proportional to the height. An alternative solution is to adopt the pin-free alignment method. For the application with frequency higher than *W*-band, or even in
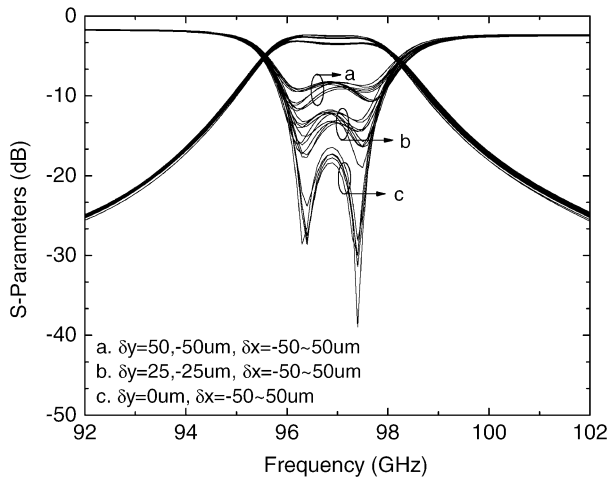
Fig. 19. Simulated filter + CPW–RWG transitions response versus frequency when layer 2 undergoes displacement.
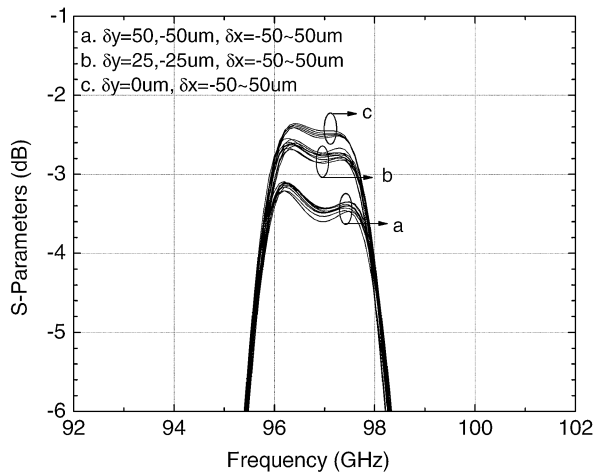

Fig. 20. Detail in the passband of simulated filter + CPW–RWG transitions response versus frequency when layer 2 undergoes displacement.

the terahertz range, the shorter wavelength makes the stacking approach easier in terms of less layers needed.

The surface roughness on waveguide sidewalls comes from the DRIE process. The conductivity is lowered by the increase of surface roughness. The surface roughness, although hard to avoid, can be further reduced by adjusting the fabrication parameters such as the power, time, and flow of the gases in the etching and passivation cycles. The other possible reason for the additional loss is the gap between the stacking wafers. Instead of cutting the waveguide along the center of the broad wall, the stacking technique may break current along the sidewall if a gap exists. In our experiment, a metal cover with four screws is used to tight the stacking wafers up. In the future, the thermal bonding technique will be employed to prevent it from gap.

VI. Conclusion

This paper has presented a novel CPW to RWG transition as an integration enabling structure for a W-band filter. The proposed transition has several advantages: the CPW and RWG are patterned and integrated on the same side of the substrate; the

coupling probe is patterned on the substrate instead of being fabricated separately. These changes make the transition more suitable for RF packaged circuits and easily extendable to terahertz applications compared to the existing transitions. The metallized probes in the proposed filter design are adopted to couple the signal from the CPW line to the waveguide resonant cavities of a two-pole filter and eliminate the need for waveguide input/output ports. In the future, the advanced compact filters can be implemented using the proposed transition.
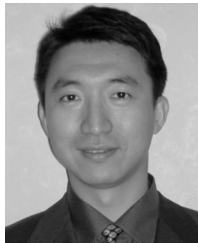
REFERENCES

[1] Q. Xiao, Y. Duan, J. L. Hesler, T. W. Crowe, and R. Weikle, "A 5-mW and 5% efficiency 210 GHz InP-based heterostructure barrier varactor quintupler," *IEEE Microw. Wireless Compon. Lett.*, vol. 14, no. 4, pp. 159–161, Apr. 2004.

[2] A. Maestrini, J. S. Ward, J. J. Gill, H. S. Javadi, E. Schlecht, C. Tripon-Canseliet, G. Chattopadhyay, and I. Mehdi, "A 540–640-GHz high-efficiency four-anode frequency tripler," *IEEE Trans. Microw. Theory Tech.*, vol. 53, no. 9, pp. 2835–2843, Sep. 2005.

[3] P. L. Kirby, D. Pukala, H. Manohara, I. Mehdi, and J. Papapolymerou, "Characterization of micromachined silicon rectangular waveguide at 400 GHz," *IEEE Microw. Wireless Compon. Lett.*, vol. 16, no. 6, pp. 366–368, Jun. 2006.

[4] G. E. Ponchak and R. N. Simons, "A new rectangular waveguide to coplanar waveguide transition," in *IEEE MTT-S Int. Microw. Symp. Dig.*, Dallas, TX, May 8–10, 1990, vol. 1, pp. 491–492.

[5] E. M. Godshalk, "A V-band wafer probe using ridge-trough waveguide," *IEEE Trans. Microw. Theory Tech.*, vol. 39, no. 12, pp. 2218–2228, Dec. 1991.

[6] R. N. Simons, "New channelized coplanar waveguide to rectangular waveguide post and slot couplers," *Electron. Lett.*, vol. 27, no. 10, pp. 856–857, May 1991.

[7] D. Deslandes and K. Wu, "Integrated microstrip and rectangular waveguide in planar form," *IEEE Microw. Wireless Compon. Lett.*, vol. 11, no. 2, pp. 68–70, Feb. 2001.

[8] N. Jain and N. Kinayman, "A novel microstrip mode to waveguide mode transformer and its applications," in *IEEE MTT-S Int. Microw. Symp. Dig.*, May 2001, pp. 623–626.

[9] D. Deslandes and K. Wu, "Analysis and design of current probe transition from grounded coplanar to substrate integrated rectangular waveguides," *IEEE Trans. Microw. Theory Tech.*, vol. 53, no. 8, pp. 2487–2494, Aug. 2005.

[10] D. Deslandes and K. Wu, "Integrated transition of coplanar to rectangular waveguides," in *IEEE MTT-S Int. Microw. Symp. Dig.*, May 2001, pp. 619–622.

[11] Y. Huang, K.-L. Wu, and M. Ehlert, "An integrated LTCC laminated waveguide-to-microstrip line T-junction," *IEEE Microw. Wireless Compon. Lett.*, vol. 13, no. 8, pp. 338–339, Aug. 2003.

[12] J. H. Lee, N. Kidera, S. Pinel, J. Papapolymerou, J. Laskar, and M. M. Tenzeris, "Comparative study of feeding techniques for 3-D cavity resonators," *IEEE Trans. Adv. Packag.*, vol. 30, no. 1, pp. 115–123, Feb. 2007.

[13] Y. Huang and K.-L. Wu, "A broadband LTCC integrated transition of laminated waveguide to air-filled waveguide for millimeter-wave applications," *IEEE Trans. Microw. Theory Tech.*, vol. 51, no. 5, pp. 1613–1617, May 2003.

[14] Y. Lee, J. P. Becker, J. R. East, and L. P. B. Katehi, "A micromachined finite coplanar line-to-silicon micromachined waveguide transition for millimeter and submillimeter wave applications," in *IEEE MTT-S Int. Microw. Symp. Dig.*, 2002, pp. 1871–1874.

[15] Y. Lee, J. P. Becker, J. R. East, and L. P. B. Katehi, "Fully micro-machined finite-ground coplanar line-to-waveguide transitions for *W*-band applications," *IEEE Trans. Microw. Theory Tech.*, vol. 52, no. 3, pp. 1001–1007, Mar. 2004.

[16] Y. Li, B. Pan, M. M. Tentzeris, and J. Papapolymerou, "A fully mi-cromachined *W*-band coplanar waveguide to rectangular waveguide transition," in *IEEE MTT-S Int. Microw. Symp. Dig.*, Jun. 2007, pp. 1031–1034.

[17] R. E. Collin, *Foundation for Microwave Engineering*, 2nd ed. New York: McGraw-Hill, 1992, p. 281.

[18] I. A. Eshrah, A. A. Kishk, A. B. Yakovlev, and A. W. Glisson, "Equiva-lent circuit model for a waveguide probe with application to DRA exci-tation," *IEEE Trans. Antennas Propag.*, vol. 54, no. 5, pp. 1433–1441, May 2006.

[19] W. W. Mumford, "The optimum piston position for wideband coaxial-to-waveguide transducers," *Proc. IRE*, vol. 41, no. 2, pp. 256–261, Feb. 1953.

[20] C. Lugo and J. Papapolymerou, "Planar realization of a triple-mode bandpass filter using a multi-layer configuration," *IEEE Trans. Microw. Theory Tech.*, vol. 55, no. 2, pp. 296–301, Feb. 2007.

[21] J. A. Ruiz-Cruz, M. El Sabbagh, K. A. Zaki, and J. M. Rebollar, "Full wave design of canonical ridge waveguide filters," in *IEEE MTT-S Int. Microw. Symp. Dig.*, 2004, pp. 603–606.

[22] J. Gipprich, D. Stevens, M. Hageman, A. Piloto, K. A. Zaki, and Y. Rong, "Embedded waveguide filters for microwave and wireless appli-cations using cofired ceramic technologies," in *Proc. Int. Microelec-tron. Symp.*, San Diego, CA, 1998, pp. 23–26.

[23] Y. Rong, K. A. Zaki, M. Hageman, D. Stevens, and J. Gipprich, "Low temperature cofired ceramic (LTCC) ridge waveguide bandpass chip filters," *IEEE Trans. Microw. Theory Tech.*, vol. 47, no. 2, pp. 2317–2324, Feb. 1999.

[24] M. El Sabbagh, H.-T. Hsu, and K. A. Zaki, "Full-wave optimization of stripline tapped-in ridge waveguide bandpass filters," in *IEEE MTT-S Int. Microw. Symp. Dig.*, Jun. 2002, pp. 1805–1808.

[25] S. Amari, "Sensitivity of coupled resonator filters," *IEEE Circuits Syst. II, Analog Digit. Signal Process.*, vol. 47, no. 10, pp. 1017–1022, Oct. 2000.
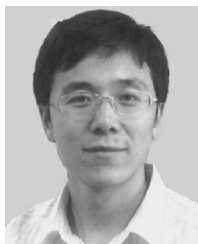
Cesar Lugo (S'01–A'02–M'06) received the B.S. degree and M.S. degree in electrical and computer engineering from the Georgia Institute of Tech-nology, Atlanta, in 2002 and 2003, respectively, and is currently working toward the Ph.D. degree in electrical engineering at the Georgia Institute of Technology.

He has developed several synthesis and design techniques for reconfigurable RF/millimeter-wave components such as filters, antennas, couplers, phase shifters, and impedance tuners. He has authored or coauthored over 15 scientific papers in peer-reviewed journals and conferences. His research interests also include hybrid semiplanar design of microwave components and adaptive algorithms for electromagnetic simulation.

Yuan Li (S'05) received the B.S. degree in automatic control from Northwestern Polytechnical University, Xi'an, China, in 1994, the M.S. degree in automatic control from the Nanjing University of Aeronautics and Astronautics, Nanjing, China, in 1997, the M.S. degree in electrical engineering from the Georgia In-stitute of Technology, Atlanta, in 2004, and is cur-rently working toward the Ph.D. degree in electrical and computer engineering at the Georgia Institute of Technology.

He was an Electronic and RF Engineer in industry. He is currently a Research Assistant with the MiRCTECH Research Group, Georgia Electronic Design Center (GEDC), Georgia Institute of Technology, Atlanta. His research interests include the development and characterization of micromachined circuits for millimeter-wave and terahertz applications, pack-aging technology for millimeter-wave systems, and passive and active circuits for wireless systems.

Mr. Li was the recipient of the 2007 IEEE Microwave Theory and Techniques Society (IEEE MTT-S) Graduate Fellowship Award.

Manos Tentzeris (S'89–M'98–SM'03) received the Diploma degree in electrical and computer engineering from the National Technical University of Athens, Athens, Greece, in 1992, and the M.S. and Ph.D. degrees in electrical engineering and computer science from The University of Michigan at Ann Arbor, in 1993 and 1998, respectively.

He is currently an Associate Professor with the School of Electrical and Computer Engineering, Georgia Institute of Technology, Atlanta. He has authored or coauthored over 260 papers in refereed journals and conference proceedings, two books, and ten book chapters. He has helped develop academic programs in highly integrated/multilayer packaging for RF and wireless applications, microwave microelectromechanical systems (MEMS), system-on-package (SOP) integrated antennas and adaptive numer-ical electromagnetics (finite difference time domain (FDTD), multiresolution algorithms), and heads the ATHENA Research Group (15 researchers). He is the Georgia Institute of Technology National Science Foundation (NSF) Pack-aging Research Center Associate Director for RF Research and the RF Alliance Leader. He is also the leader of the Novel Integration Techniques Subthrust of the Broadband Hardware Access Thrust of the Georgia Electronic Design Center (GEDC) of the State of Georgia. During the summer of 2002, he was a Visiting Professor with the Technical University of Munich, Munich, Germany, where he introduced a course in the area of high-frequency packaging. He has given over 40 invited talks in the same area to various universities and companies in Europe, Asia, and the U.S.

Dr. Tentzeris is a member of URSI Commission D, an associate member of the European Microwave Association (EuMA), and a member of the Technical Chamber of Greece. He was the 1999 Technical Program co-chair of the 54th ARFTG Conference, Atlanta, GA, and he is the vice-chair of the RF Technical Committee (TC16) of the IEEE Components, Packaging, and Manufacturing Technology (CPMT) Society. He has organized various sessions and workshops on RF/Wireless Packaging and Integration in IEEE ECTC, IMS, and AP-S Sympo-sia, for all of which he is a member of the Technical Program Committee in the area of components and RF. He was the recipient of the 2003 National Aero-nautics and Space Administration (NASA) Godfrey "Art" Anzic Collaborative Distinguished Publication Award for his activities in the area of finite-ground low-loss low-crosstalk CPWs, the 2003 IBC International Educator of the Year Award, the 2003 IEEE CPMT Outstanding Young Engineer Award for his work on 3-D multilayer integrated RF modules, the 2002 International Conference on Microwave and Millimeter-Wave Technology Best Paper Award (Beijing, China) for his work on compact/SOP-integrated RF components for low-cost high-performance wireless front-ends, the 2002 Georgia Institute of Technology Electrical and Computer Engineering Outstanding Junior Faculty Award, the 2001 ACES Conference Best Paper Award, the 2000 NSF CAREER Award for his work on the development of multiresoluation time-domain (MRTD) tech-nique that allows for the system-level simulation of RF integrated modules, and the 1997 Best Paper Award of the International Hybrid Microelectronics and Packaging Society for the development of design rules for low-crosstalk finite-ground embedded transmission lines. He was the recipient/corecipient of the 2007 IEEE AP-S Symposium Best Student Paper Award, the 2007 IEEE IMS Third Best Student Paper Award, the 2007 ISAP 2007 Second Best Poster Pre-sentation Award, the 2006 IEEE MTT-S Outstanding Young Engineer Award, and the 2006 Asia–Pacific Microwave Conference Award.

Bo Pan (S'03) received the B.S. degree (with honors) and M.S. degree (with honors) from Ts-inghua University, Beijing, China, in 2000 and 2003 respectively, and is currently working toward the Ph.D. degree in electrical and computer engineering at the Georgia Institute of Technology, Atlanta.

He was a Visiting Scholar with Microsoft Re-search Asia prior to joining the Georgia Institute of Technology, in August 2003. He is currently a Graduate Research Assistant with the ATHENA Research Group and MiRCTECH Research Group, Georgia Institute of Technology. He is a Research Member of the Georgia Electronic Design Center (GEDC) and GT-NSF Packaging Research Center (PRC). His research involves the design, processing, and characterization of components and circuits for RF/microwave/millimeter-wave transmit/receive (T/R) modules with a focus on micromachining technologies. He is also involved with research on antenna designs for multiple wireless applications.

John Papapolymerou (S'90–M'99–SM'04) received the B.S.E.E. degree from the National Technical University of Athens, Athens, Greece, in 1993, and the M.S.E.E. and Ph.D. degrees from The University of Michigan at Ann Arbor, in 1994 and 1999, respectively.

From 1999 to 2001, he was an Assistant Professor with the Department of Electrical and Computer Engineering, University of Arizona, Tucson. During the summers of 2000 and 2003, he was a Visiting Professor with the University of Limoges, Limoges, France. From 2001 to 2005, he was an Assistant Professor with the School of Electrical and Computer Engineering, Georgia Institute of Technology, Atlanta, where he is currently an Associate Professor. He has authored or coauthored over 140 publications in peer-reviewed journals and conferences. His research interests include the implementation of micromachining techniques and MEMS devices in microwave, millimeter-wave and terahertz circuits and the development of both passive and active planar circuits on semiconductor (Si/SiGe, GaAs) and organic substrates (liquid-crystal polymer (LCP), LTCC) for system-on-a-chip (SOC)/system-on-package (SOP) RF front ends.

Dr. Papapolymerou is the vice-chair for Commission D of the U.S. National Committee of URSI. He is an associate editor for IEEE MICROWAVE AND WIRELESS COMPONENT LETTERS and the IEEE TRANSACTIONS ON ANTENNAS AND PROPAGATION. During 2004, he was the chair of the IEEE Microwave Theory and Techniques (MTT)/Antennas and Propagation (AP) Atlanta Chapter. He was the recipient of the 2004 Army Research Office (ARO) Young Investigator Award, the 2002 National Science Foundation (NSF) CAREER Award, the Best Paper Award presented at the 3rd IEEE International Conference on Microwave and Millimeter-Wave Technology (ICMMT2002), Beijing, China, and the 1997 Outstanding Graduate Student Instructional Assistant Award presented by the American Society for Engineering Education (ASEE), The University of Michigan at Ann Arbor Chapter. His student was also the recipient of the Best Student Paper Award presented at the 2004 IEEE Topical Meeting on Silicon Monolithic Integrated Circuits in RF Systems, Atlanta, GA.